Photoelectrochemical properties of sol-gel and particulate TiO_2 layers

Georg Waldner,[1] Josef Krýsa,[2] Jaromír Jirkovský,[3] and Gottfried Grabner[4]

[1] *Institute of Materials Chemistry, Vienna University of Technology, Veterinaerplatz 1, A-1210 Vienna, Austria*

[2] *Institute of Chemical Technology, Department of Inorganic Technology, Technická 5, 166 28 Prague 6, Czech Republic*

[3] *J. Heyrovský Institute of Physical Chemistry, Academy of Sciences of the Czech Republic, Dolejškova 3, 182 23 Prague 8, Czech Republic*

[4] *Institute for Theoretical Chemistry and Structural Biology, University of Vienna Dr. Bohrgasse 7b, A-1030 Vienna, Austria*

ABSTRACT. Polarization curves on irradiated TiO_2 layers were measured in various electrolytes, namely sodium hydroxide, sulphuric acid, oxalic acid and potassium oxalate. Photocurrents measured in 0.1 M NaOH are very small and decrease with increasing number of Degussa P25 TiO_2 layers. Photocurrents for sol-gel TiO_2 layers in 0.1 M NaOH are about five times higher than for P25 TiO_2 layers and increasing with number of layers. The same holds for Na_2SO_4, but in H_2SO_4 the difference between P25 and sol-gel diminishes, however the sol-gel layers still show the higher currents. In solutions of oxidizable substrates the trend is inversed: P25 layers show higher currents, with a steep increase with concentration of solute. The shape of the polarization curves was interpreted in terms of response time to irradiation and photocurrent depletion. Degradation experiments demonstrated that the effect (and advantage) of biasing the electrode depends on adsorption properties of substance and surface area of electrode material.

1. INTRODUCTION

The aim of the paper is the comparison of photoelectrochemical properties of various TiO_2 layers, namely particulate, sol-gel and thermally produced layers. Recombination of photogenerated positive holes and electrons inside semiconductor particles is generally responsible for a relatively low quantum yield of the photocatalytic degradation. A possible way to increase the electron-hole separation and consequently to enhance quantum yield is the application of a potential bias.

Conventional semiconductor theory essentials postulate the formation of a depletion layer in a doped semiconductor having sufficiently "large particles". The generation of a depletion layer requires the transfer of mobile charge carriers between the semiconductor and the electrolyte. When an electroactive species is present in the electrolyte the charge transfer can take place directly across the semiconductor-solution interface. Alternatively, in the absence of a suitable redox couple in the solution, the semiconductor can be polarized by applying an external bias voltage across the junction via an ohmic contact mounted at the backside of the electrode [1]. This photoelectrochemical effect of application of a potential to a TiO_2 film was recently illustrated in detail by Butterfield *et al.* [2]. There are numerous works describing the photoelectrochemical properties of such TiO_2 films [3–6]. The positive effect of imposed bias on the decomposition of organics has also been reported [6–8]. The variety of sol-gel methods is shown in [9].

Another approach represents the use of *particulate* films with highly porous structure [5, 6, 10–13]. The porosity of the film is a film property and not determined by the particles, which are non-porous themselves: P25 is a non-porous 70 : 30% anatase/rutile mixture with a BET surface area of $55 \pm 12\,m^2\,g^{-1}$ and crystallite sizes of 30 nm in 0.1 μm diameter aggregates. Vinodgopal *et al.* [10] used a particulate film prepared by spreading a P25 TiO_2 slurry onto conducting glass and drying it at 400 °C. Hagfeld *et al.* [5] and Mbindyo *et al.* [6] prepared a nanocrystalline film by preparing a viscous suspension of P25 TiO_2 in a mixture of water with acetyl acetone; it was spread onto conducting glass, then dried in air and heated at 600 °C. Byrne *et al.* [12] used electrophoretic coating of a Ti alloy substrate, using a suspension of P25 TiO_2 in methanol.

Small particle size (such as found in Degussa P25) precludes the formation of a depletion layer as such across the layer due to inter-particle boundaries, and so the observed photoelectrochemistry is determined by the relative rates of capture of holes and electrons

at the surface of the particles. An effect of electrode potential under these conditions can be ascribed to electrophoretic drift of electrons to the back contact of the photoanode. Thus one can also minimize charge recombination by application of an anodic bias to the particulate TiO_2 film. Application of this simple concept of achieving better charge separation in particles is important for improving the efficiency of photocatalytic degradation of organic contaminants, partially compensating for the mass transfer problems connected with the use of semiconductor thin films.

2. EXPERIMENTAL

2.1. Chemicals. Diisopropoxytitanium(IV)bis(acetylacetonate) (75% (v/v) solution in isopropanol), oxalic acid (> 99%): Fluka; 4-chlorophenol (> 98%), formic acid: Merck-Schuchardt; acetonitrile: Riedel-de-Haën CHROMASOLV (HPLC grade); monuron: Sigma-Aldrich. Conducting glass substrates: F : SnO_2 (Solems, France), sheet resistivity: 10 Ohms/square. Water was purified by a Millipore Simplicity 185 ultra pure water equipment.

2.2. Analytical. For total organic carbon (TOC) analyses a Shimadzu TOC 5000 analyzer equipped with an autosampler ASI 5000 was used. TOC was determined as the difference between total carbon (TC, via catalytic oxidation at 680 °C) and inorganic carbon (IC, acidification by phosphoric acid).

The HPLC system consisted of the following parts: isocratic pump (Spectra Physics Isochrom LC Pump); UV-VIS detector (Spectra Physics, Spectra 200 programmable wavelength detector); column (Merck LiChroCART R 250-4 HPLC_Cartridge LiChrospher R 100 RP-18 (5 μm)); pre-column (LiChroCART R 4-4 LiChrospher R 100 RP-18 (5 μm)).

2.3. Production of TiO_2 electrodes. A procedure similar to Vinodgopal *et al.* [10] was used for producing the particulate electrodes: a P25 slurry (10 g/l) was spread over the SnO_2-coated glass substrate, and after a settling time of one hour the remaining solution was decanted; the electrode was then dried at 300 °C for one hour. By this fixing procedure the properties of TiO_2 P25 (Degussa) are thus preserved, in particular the temperature is sufficiently low as to prevent sintering of the particles with its associated decrease in active surface area.

In this paper a simplified sol-gel procedure was used: the precursor solvent (isopropanol) was replaced with ethanol by rotary evaporation and successive addition of ethanol to maintain the initial concentration of 75% (v/v) [14]. For this series of layers the full concentration of 2 M was used. The substrates were pretreated by washing with acetone and Millipore® water. A spin-coater (Specialty Coating Systems, SCS P6708 D) was used for coating of substrates at a rotation speed of 2000 rpm. 100 μl aliquots of the solution were applied onto the spinning substrate, the hydrolysis took place in the film under ambient conditions (purging of equipment by synthetic air, 30% rH, 22 °C). Finally, the coated samples were heated for one hour at 550 °C under atmospheric conditions.

2.4. Polarization curves. Photoelectrochemical measurements were performed using a three-compartment electrochemical cell with a Pyrex window; the volume of solution was 15 ml. The experiments were done in a 3-electrode set-up consisting of the TiO_2 working electrode, a titanium metal wire or platinum mesh acting as counter electrode and a Ag/AgCl reference electrode (3 M KCl, saturated with AgCl). Therefore all potentials mentioned in this paper are referred to this reference electrode with a potential of 216 mV *vs.* NHE.

The surface of the TiO_2 electrodes was delimited to 1 cm^2 with Teflon tape. As irradiation source a Zeiss ST41 housing with a 45 W mercury medium pressure Heraeus lamp was used, monochromatized by a 365 nm interference filter. The potential sweep was done by a home-made potentiostat as described in Popkirov [15], at a scan rate of 20 mV/s unless stated otherwise. The potential-current curves were recorded by a Keithley-Metrabyte DAS 1602 AD/DA data acquisition PC card.

A Hamamatsu S1337-1010BQ Si photodiode was used for measuring the light intensity, which was 7 mW/cm^2 at 365 nm for most experiments. However, during the last runs, which were performed later, the lamp had degraded down to 3 mW/cm^2.

3. RESULTS

Mass and gravimetrically calculated thickness of the investigated TiO_2 layers are shown in Table 1. Each layer of P25 represents about 1–1.2 mg/cm^2; on the other hand the sol-gel layers are so thin that the weight gain was not measurable.

Photoelectrochemical results are summarized in Table 2. As the UV lamp output decreased down to less than 50% of its initial value in the course of several weeks, the approach of comparing the quantum yields of photocurrent generation was chosen [14, 16]. This quantum yield, also known as IPCE = incident-photon-to-current conversion efficiency, is given by the relation

$$\mathrm{IPCE} = \frac{i}{F} \cdot \frac{1}{P} \quad \text{with } i = \text{current},$$

F = Faraday constant, P = incident Einstein/s.

3.1. Effect of pH on polarization curves. The polarization curves (from −0.8 to +0.8 V *vs.* Ag/AgCl) for P25 TiO_2 (one layer) and sol-gel TiO_2 (one layer) in 0.1 M NaOH are shown in Figure 1. Oxygen evolution starts at

Table 1. *Mass and estimated thickness of* P25 TiO_2 *layers. Electrodes 1–8:* P25*; electrodes 9–12: sol-gel.*

Electrode #	No. of layers	M (TiO_2)/mg cm^{-2}	average	thickness/μm
P25_1	1	1.22		
P25_2	1	0.88		
P25_3	1	0.96		
P25_4	1	1.04	1.02	2.7
P25_5	2	2.3		
P25_6	2	2.36	2.33	6.1
P25_7	3	3.5		
P25_8	3	3.66	3.58	9.4
SG_9	1	n.d.		
SG_10	1	n.d.		
SG_11	5	n.d.		
SG_12	5	n.d.		

Table 2. *Photocurrents and IPCEs of the investigated electrodes in different electrolytes. Potential = 0.6 V vs.* Ag/AgCl.

Electrode →	P25 1 layer		P25 2 layers		P25 3 layers		SG 1 layer		SG 5 layers	
Electrolyte	i_{ph}/A/cm^2	IPCE	i_{ph}/A/cm^2	IPCE	i_{ph}/A/cm^2	IPCE	i_{ph}/A/cm^2	IPCE	i_{ph}/A/cm^2	IPCE
0.1 M Na_2SO_4	6.10E-06	0.0061			1.70E-06	0.0017	6.73E-05	0.067		
0.1 M NaOH	1.25E-05	0.0061	1.01E-05	0.0049	4.11E-06	0.0020	6.94E-05	0.033	1.98E-04	0.096
0.05 M H_2SO_4	5.47E-05	0.027			3.29E-05	0.0160			1.03E-04	0.050

potentials positive of about 0.7 V and hydrogen evolution below −0.4 V. The IPCE for TiO_2 P25 is very small while for sol gel TiO_2 layers it is about five times higher. Then the behavior in 0.1 M Na_2SO_4 was studied; photocurrents and IPCE values are shown in Table 2. The difference in IPCE between sol-gel and P25 layers is even higher than in NaOH. Low photocurrents on P25 electrodes in pure electrolyte indicate a high recombination rate; the electrons do not reach the back contact.

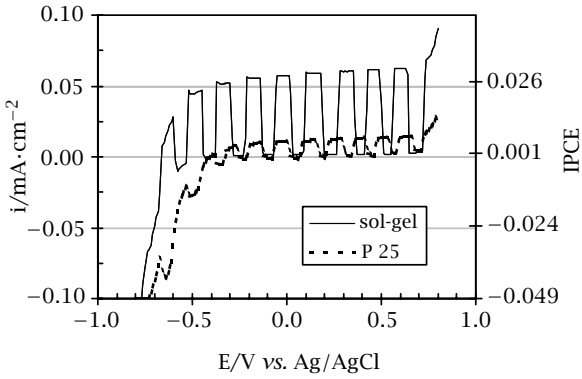

Figure 1. *Polarization curves for* P25 *(1 layer* TiO_2*) and sol-gel* TiO_2 *(one layer) on* SnO_2*; supporting electrolyte: 0.1 M* NaOH*; scan rate: 0.02 V/s, light intensity:* $2.1 \cdot 10^{-8}$ *E/s at 365 nm.*

The third step was the comparison of both layers in 0.05 M H_2SO_4 as depicted in Figure 2. It is apparent that H_2 evolution starts at about −0.2 V, which is more positive than in the case of 0.1 M NaOH. The flatband potential, which is in many cases equivalent to the open circuit potential and photocurrent onset potential, shifts with a Nernstian behavior [16]. For both electrodes we can observe a plateau photocurrent, which is independent of applied potential between 0 and 1 V.

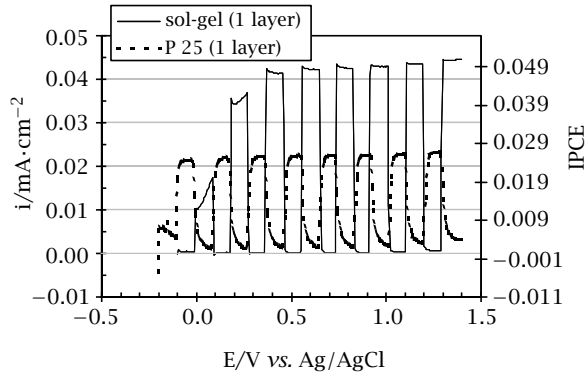

Figure 2. *Polarization curves for* P25 TiO_2 *(1 layer) sol-gel* TiO_2 *(one layer) on* SnO_2*; supporting electrolyte: 0.05 M* H_2SO_4*; scan rate: 0.01 V/s, light intensity:* $9.0 \cdot 10^{-9}$ *E/s.*

Comparing IPCEs at the potential of 0.6 V in different electrolytes, the difference between both layers in 0.05 M H_2SO_4 is much smaller than in 0.1 M NaOH. The IPCE of the sol-gel layer in 0.05 M H_2SO_4 is only slightly higher than in 0.1 M NaOH. IPCEs for the P25 layer in 0.1 M NaOH are about the same as in 0.1 M Na_2SO_4, and both are five times lower than in 0.05 M H_2SO_4. The strong increase of photocurrents on P25 electrodes in H_2SO_4 might indicate a preferential photocorrosion of nanoparticulate electrodes.

3.2. Effect of layer thickness. The layer thickness showed different effects on the photocurrent-potential behavior for the two types of layers. For the sol-gel layer, photocurrents (as measured in 0.1 M Na_2SO_4) are compared in Figure 3: an increase of photocurrent with layer thickness is observed; additionally, the five-layer electrode shows no plateau photocurrent. In Figure 4 the same type of comparison is shown for one and three layers of P25; an inverse effect of the layer thickness on the photocurrent is observed.

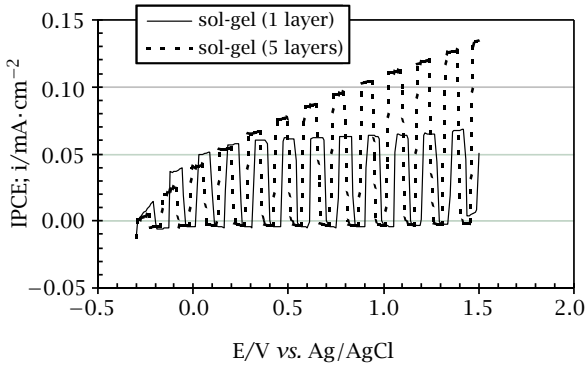

Figure 3. *Effect of layer thickness on polarization curve for sol-gel* TiO_2 *layers, supporting electrolyte: 0.1 M* Na_2SO_4*, scan rate: 0.02 V/s, light intensity:* $1.03 \cdot 10^{-8}$ *E/s.*

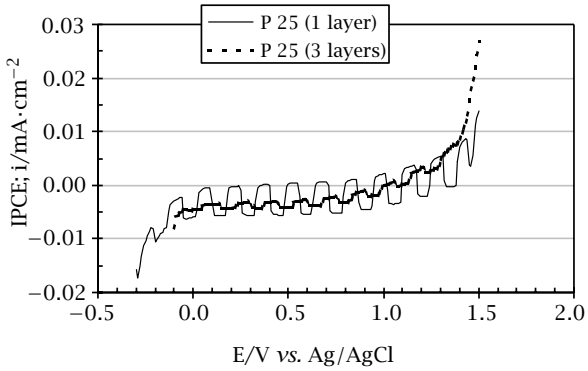

Figure 4. *Effect of layer thickness on polarization curve for* P25 TiO_2 *layers, supporting electrolyte: 0.1 M* Na_2SO_4*, scan rate: 0.02 V/s, light intensity:* $1.03 \cdot 10^{-8}$ *E/s.*

The thicker P25 layer showed a decrease in photocurrent compared to the one-layer electrode. Tentative explanation [17]: the layer has exceeded the optimum thickness. It will harvest all light, but charge carriers generated at a depth of more than the width of the depletion layer plus minority carrier diffusion length will recombine and decrease the efficiency. Another way of explanation will be the fact that too thick films show high resistivity towards electron transport to the back contact. The migration speed for electrons and holes begin to differ more and more with increasing film thickness: the holes do not have to cross the entire film as the electrolyte penetrates the pores of the film and reacts on their surfaces with the photogenerated holes. The problems with electron transport might be a consequence of the absence of particle sintering, which in turn is caused by the low annealing temperature of 300 °C.

Generally, the thicker sol-gel layer showed a higher photocurrent: this means that the process is charge-carrier limited: not all of the incident photons are collected as the optimal thickness has not been reached (the layer thickness is smaller than the depletion layer width), and upon increase of thickness the number of collected photons still increases.

Photometric measurements of optical density of the layers confirmed the concept of optimal *vs.* suboptimum layer thickness: one layer of P25 absorbs 97%, but one sol-gel layer only 30% of the incident light.

3.3. Influence of oxidizable substrate. Polarization curves for P25 layers for various $(COOH)_2$ concentrations are shown in Figure 5. Photocurrents showed a plateau from 0 to 1.5 V and an increase of the plateau current with rising concentrations. A similar increase in photocurrent was also observed in HCOOH solutions, cf. Table 2. In both substrates, the thicker layer again showed a decrease in photocurrent compared to the one-layer electrode and has been discussed above.

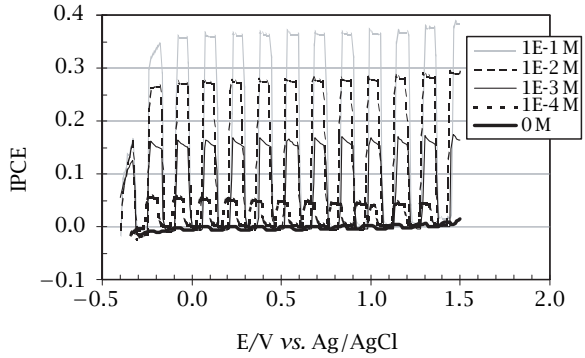

Figure 5. *Polarization curves for* P25 TiO_2 *(one layer) for various concentrations of* $(COOH)_2$*; supporting electrolyte: 0.1 M* Na_2SO_4*, scan rate: 0.02 V/s, light intensity:* $9.0 \cdot 10^{-9}$ *E/s.*

On the other hand, over the one-layer sol-gel electrode photocurrents in oxalic acid showed a plateau between 0.3 V and 1.5 V, as depicted in Figure 6. The increase of this plateau current with increase in concentration was steady but not as steep as for the P25 electrodes—as the current in pure supporting electrolyte was already high.

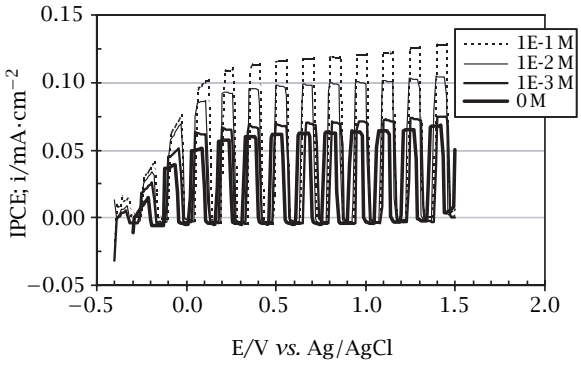

Figure 6. *Polarization curves for sol-gel* TiO_2 *(one layer) for various concentrations of* $(COOH)_2$*; supporting electrolyte: 0.1 M* Na_2SO_4*, scan rate: 0.02 V/s, light intensity:* $1.03 \cdot 10^{-8}$ *E/s.*

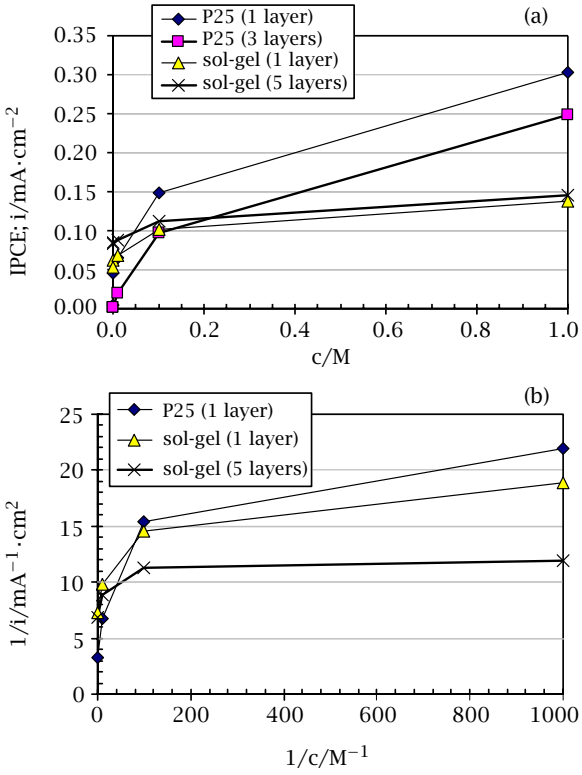

Figure 7. *Concentration dependence of photocurrent in* HCOOH *at 0.6 V vs.* Ag/AgCl*; supporting electrolyte: 0.1 M* Na_2SO_4*, scan rate: 0.02 V/s, light intensity:* $1.0 \cdot 10^{-8}$ *E/s.*

The dependence of photocurrents (at a fixed potential of 0.6 V *vs.* Ag/AgCl) for P25 and sol-gel layers on the concentration of $(COOH)_2$ and HCOOH is shown in Figures 7 and 8, respectively. In the case of $(COOH)_2$ the photocurrent for the sol-gel layer increases only slightly with concentration, whereas for the P25 layer there is a sharp rise, starting from virtually zero (photocurrent) in pure supporting electrolyte. For HCOOH

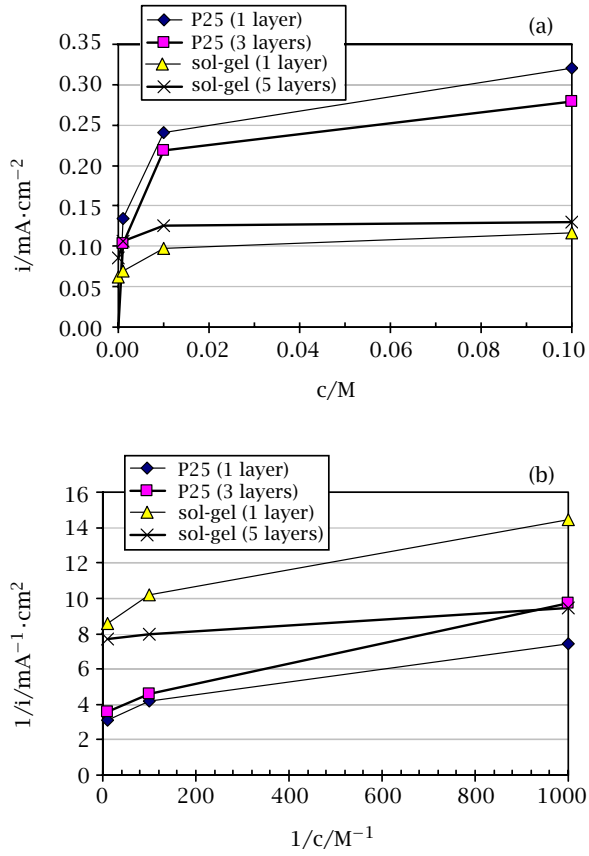

Figure 8. *Concentration dependence of photocurrent in* $(COOH)_2$ *at 0.6 V vs.* Ag/AgCl*; supporting electrolyte: 0.1 M* Na_2SO_4*, scan rate: 0.02 V/s.*

the shape of photocurrent-concentration dependence is qualitatively similar to oxalic acid with the exception of a significant shift of photocurrent for P25 electrodes: in other words, on P25, formic acid has to be at a one order higher concentration than oxalic acid to yield the same photocurrent. It is interesting that unlike in oxalic acid, photocurrents for P25 and sol-gel layers in HCOOH are quite similar for intermediate concentrations (10^{-3} and 10^{-2} M).

A representation accounting for the expected Langmuir-Hinshelwood adsorption mechanism was chosen: if the photocurrent was analogous to initial reaction rate, a linear behavior of a plot $1/i = 1/k + 1/c_0$ could be expected. This can be confirmed for oxalic acid (Figure 8(b)), but not for formic acid (Figure 7(b)).

Generally, a steep increase of photocurrent with concentration of oxidizable substrate can be attributed to current doubling: after a first oxidation step, the oxidized intermediate can inject an electron into the conduction band of TiO_2 (second oxidation step). The adsorbate helps reducing the recombination by enhancing the reaction rate with holes.

Table 3. *Summary of degradation experiments done over the investigated electrodes; $J_{org}/J_{h\nu}$ = quantum yield.*

substrate	E/V (Ag/AgCl)	photon flux/ E cm^{-2} s^{-1}	time/min	Δc/M	degr. flux/ mol cm^{-2} s^{-1}	$J_{org}/J_{h\nu}$	increase with bias/%
P 25, 1 layer							
4-CP, 0.5 mM	Eoc = −0.1	1.38E-08	1015	2.17E-04	5.34E-11	0.0039	
4-CP, 0.5 mM	0.6	1.37E-08	1015	2.42E-04	5.96E-11	0.0044	13.0
sol-gel, 1 layer							
4-CP, 0.5 mM	Eoc = −0.24	9.01E-09	985.2	4.20E-05	1.07E-11	0.0012	
4-CP, 0.5 mM	0.6	9.01E-09	975	2.09E-04	5.36E-11	0.0059	403
				ΔTOC/mg/l			
P 25, 1 layer							
OA, 5 mM	Eoc = −0.57	1.05E-08	900	61.4	7.11E-10	0.068	
OA, 5 mM	0.6	1.04E-08	310	48.3	1.62E-09	0.156	130
sol-gel, 1 layer							
OA, 5 mM	Eoc = −0.53	9.30E-09	575	8.2	1.49E-10	0.016	
OA, 5 mM	0.6	9.30E-09	300	19.3	6.70E-10	0.072	351

3.4. Response time and photocurrent depletion. Two other interesting features of the photocatalytically active layers are the time of response to light and the depletion of the photocurrent with time of irradiation.

P25 layers show a high response time to irradiation, while sol-gel layers show a quick response (cf. Figures 3 and 4), giving an indication about the lower charge carrier migration speed in P25 layers.

On the other hand, the depletion of the photocurrent signal is inversely proportional to the concentration of oxidizable contaminant, see Figure 5. This holds only for one layer of P25, because with three layers this effect is superimposed by the slow response to irradiation.

Similar observations were reported concerning photocurrent instability in unbuffered solutions [11]. This photocurrent depletion has been postulated [12] as being due to a depletion of the Helmholtz layer in oxalate after an initial current spike, therefore the oxidation of water and the electron-hole recombination become more probable and thus decrease the probability of electrons reaching the back contact. The higher the concentration, the quicker the oxalate-depleted region will be replenished, hence the less pronounced decay in photocurrent.

3.5. Photocatalytic activity in degradation experiments. The investigation of the electrodes' behavior in the mentioned electrolytes was then extended with respect to the mineralization of the oxidizable substrates, i.e. their oxidation to inorganic substances. The degradation experiments are presented in Table 3; $J_{org}/J_{h\nu}$ represents the external quantum yield (referring to incident photons). Notice the different behavior towards biasing the electrodes, depending on adsorption properties of the substance:

At open circuit, both layers show identical performance for 4-CP degradation (little adsorption onto TiO_2), taking account of the absorbed amount of light (30% absorbed by the sol-gel layer, 97% by the P25 layer). For the strongly adsorbing substrate (oxalic acid), the larger surface area of P25 is favorable and leads to good degradation results even without any bias (compare to 18, 19, 20).

A bias of 0.6 V increases the reaction rate by 350–400% (sol-gel), independently of adsorption properties of the substance. P25 cannot efficiently be biased without adsorbing substrate because of high electron transport resistance in the porous layer; it works already at open circuit. P25 can be biased in presence of an adsorbing substrate (oxalic acid), leading to a high increase in reaction rate.

3.6. Open circuit potentials. The open circuit potential (Eoc) reflects charging effects upon dissociative adorption and reaction of species on the interface semiconductor | electrolyte. The changes in open circuit potential when switching from dark to light are shown in Figure 9. For both types of layer there is a negative shift when the TiO_2 layer is irradiated. This is due to the fact that photogenerated holes react faster with water on the surface of TiO_2 particles, forming

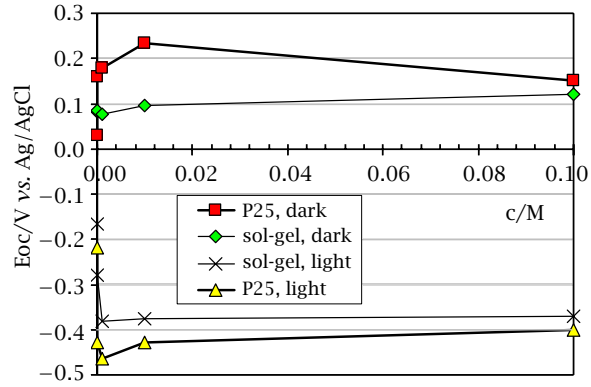

Figure 9. *Open circuit potentials as a function of oxalic acid concentration. Note the maximum in dark and minimum under irradiation.*

OH radicals. Photogenerated electrons remain in the TiO_2 particles and charge them negatively. Thus we can assume that with increasing negative shift the steady state concentration of electrons increases. The Eoc for P25 is about 50 mV lower than for sol gel. This might be due to the higher surface area of particulate layers and the higher amount of adsorbed water, yielding a higher steady state concentration of OH radicals on the surface.

When an oxidizable substrate is present, the Eoc is shifted even more negative. This means that a higher amount of photogenerated holes react with organic substrate and therefore the photostationary concentration of electrons is higher.

In the case of sol-gel layer the negative shift was observed for all substrates (slightly smaller for 4-CP), and Eoc decreased with increasing substrate concentration.

For P25 layer the negative shift was observed only in oxalic and formic acid. In presence of formic acid Eoc decreases with concentration while in oxalic acid there is a strong increase in Eoc already at a concentration of 10^{-4} M, and with increasing concentration the value of Eoc is stable. In the presence of 4-CP there is a negative shift when switching on the light, but Eoc values at light are—for all 4-CP concentrations—lower than without 4-CP.

This implies that the values of Eoc for particulate layers depend on the adsorption affinity of substrates to the TiO_2 surface. Oxalic acid is strongly adsorbed on TiO_2 and reacts directly with holes. The adsorption of 4-CP is much lower. A particulate layer has a much higher surface area than a sol gel layer. Therefore adsorption properties of oxidizable substrates to sol-gel TiO_2 do not play an important role.

4. CONCLUSIONS

TiO_2 thin films were synthesized on conducting glass substrates via deposition from P25 slurries and via a simplified sol-gel route. These electrodes were compared by observing their polarization curves in various electrolytes: Na_2SO_4, NaOH, H_2SO_4. In these pure electrolytes, P25 electrodes showed lower photocurrents than sol-gel TiO_2.

The addition of oxidizable substrates (oxalic acid, formic acid, 4-chlorophenol) lead to higher photocurrents for P25 than sol-gel TiO_2; currents increase with substrate concentration. This was interpreted in terms of current doubling effect.

P25 electrodes showed a slow response to light signals (in contrast to sol-gel electrodes with their instantaneous reaction), and their photocurrent decreased to a steady-state current in solutions of oxidizable substrate of low concentration.

Degradation reactions of model wastewaters showed a different benefit from application of a positive voltage to the electrodes: P25 electrodes work quite well at open circuit potential, whereas the sol-gel electrodes' performance exhibits an enormous improvement by application of a bias.

Open circuit potentials illustrate the charging effect of the electrolyte/catalyst interface.

ACKNOWLEDGEMENTS

This project was financially supported by the Czech grant agency (203/02/0983), project KONTAKT 2000/15, KONTAKT 2002/11 and the European commission, project ABWAS2 (contract ICA3-CT-1999-00016). We would also like to express our thanks to Dr. Michael Neumann-Spallart for a lot of fruitful discussions.

GLOSSARY

4-CP	4-Chlorophenol
Eoc	open circuit potential
FA	formic acid
OA	oxalic acid
SG	sol-gel
TOC	total organic carbon [mg/l]

REFERENCES

[1] M. Grätzel, Heterogeneous photochemical electron transfer, CRC Press, 1989.
[2] I. M. Butterfield, P. A. Christensen, A. Hamnett, K. E. Shaw, G. M. Walker, and S. A. Walker, J. Appl. Electrochem. **27** (1997), 385.
[3] L. Kavan and M. Grätzel, Electrochim. Acta **40** (1995), 643.
[4] Y. Hamasaki, S. Ohkubo, K. Murakami, H. Sei, and G. Nogami, J. Electrochem. Soc. **141** (1994), 660.
[5] A. Hagfeldt, H. Lindstrom, S. Sodergren, and S.-E. Lindquist, J. Electroanal. Chem. **381** (1995), 39.
[6] J. K. N. Mbindyo, M. F. Ahmadi, and J. F. Rusling, J. Electrochem. Soc. **144** (1997), 3153.
[7] D. H. Kim and M. A. Anderson, Environ. Sci. Tech. **28** (1994), 479.
[8] P. Fernández-Ibáñez, S. Malato, and O. Enea, Catal. Today **54** (1999), 329.
[9] J. Livage, C. Sanchez, M. Henry, and S. Doeff, Solid State Ionics **32/33** (1989), 633.
[10] K. Vinodgopal, S. Hotchandani, and P. V. Kamat, J. Phys. Chem. **97** (1993), 9040.
[11] K. Vinodgopal, U. Stafford, K. A. Gray, and P. V. Kamat, J. Phys. Chem. **98** (1994), 6797.
[12] J. A. Byrne and B. R. Eggins, J. Electroanal. Chem. **457** (1998), 61.
[13] J. A. Byrne, B. R. Eggins, N. M. D. Brown, B. McKinney, and M. Rouse, Applied Catalysis B: Environmental **17** (1998), 25.
[14] M. Neumann-Spallart, private communication (2001).

[15] G. S. Popkirov and R. N. Schindler, Review of Scientific Instruments, **63**(11) (1992), 5366.

[16] H. O. Finklea, Studies in Physical and Theoretical Chemistry, vol. **53**, 1988, chapter 2, pp. 43–145.

[17] H. T. Chang, N. M. Wu, and F. Zhu, Water Research **34**(2) (1999), 407.

[18] J. Kulas, I. Roušar, J. Krýsa, and J. Jirkovský, J. Appl. Electrochem. **28** (1998), 843.

[19] J. Krýsa, L. Vodehnal, and J. Jirkovský, J. Appl. Electrochem. **29** (1999), 429.

[20] J. Krýsa, K. Bouzek, and Ch. Stollberg, J. Appl. Electrochem. **30** (2000), 1033.